Thin Solid Films 777 (2023) 139894

Contents lists available at ScienceDirect

Thin Solid Films

journal homepage: www.elsevier.com/locate/tsf

Gold coated vertically aligned carbon nanotubes as electrode for electrochemical capacitors

Sabrina Roguai [a,b,*], Abdelkader Djelloul [a,b]

[a] LASPI2A Laboratory of Structures, Properties and Interatomic Interactions, Abbes Laghrour University, Khenchela 40000, Algeria
[b] Science of Matter, Abbes Laghrour University, Khenchela 40000, Algeria

ARTICLE INFO

Keywords:
Gold
Carbon nanotubes
Vertically aligned carbon nanotubes
Electrochemical capacitors
Cyclic voltammetry

ABSTRACT

In this work, gold (Au) films were deposited onto vertically aligned carbon nanotubes (CNTs) by Dc magnetron sputtering method for use as super-capacitor electrodes. By so doing, we synthesize a porous Au deposit anchored on the CNTs with a high apparent surface area. The structure and microstructure studies revealed that the Au@CNTs have a porous nanostructure morphology. The porous Au/CNTs electrodes exhibit an a good areal capacitance compared to state of art Au based electrode (25.6 mF cm^{-2} at 5 $mV.s^{-1}$) and excellent cycling stability (90% retention after 10.000 cycles) in 0.5 M H_2SO_4 aqueous solution. These results demonstrate the beneficial use of CNTs to fabricate a porous Au deposit with improved electrochemical energy storage. In addition, these porous structures can also be used as templates for another type of materials for electrochemical energy storage.

1. Introduction

Among the various energy storage systems, electrochemical capacitors (ECs) also called supercapacitors have attracted increasing attention as potential candidates for energy storage, due to their high power density and long cycle life [1–3]. Carbon materials such as graphene [4,5], activated carbon [6–9], carbon nanotube (CNT) [10,11], carbide-derived carbons [12,13], mesoporous carbon [14,15], and carbon aerogel [16–18], are widely used as promising materials for supercapacitors, or templates for different material deposition because of their high surface area, excellent conductivity, and electrochemical stability [19–24]. A supercapacitor using CNT-forest transferred onto an elastomeric substrate with assistance from a thermal annealing process in an atmospheric environment was unveiled by Changyong et al. [25]. This CNT-forest electrode exhibited excellent electrochemical performance as well as high stability under either uniaxial (300%) or biaxial (300% × 300%) stresses under thousands of stretch-relaxation cycles. On the other hand, Sheng et al. [26], through the design of 3D electrodes, a substantial improvement in vertical 3D nanomaterial based systems for energy storage at the microscopic scale device

Gold (Au) with high content has also been used as a model for the deposition of transition metal oxides in order to improve the electrical conductivity of the deposited material. Thanks to these properties work based on the combination of Au and CNT in order to allow the optimization of their single properties to create systems that are potentially versatile [27]. However, report on porous Au as electrode for ECs is scarily reported in literature. For example as it permits the integration of their own unique properties in order to achieve potentially multipurpose systems. Au electrodeposition on CNT tips has been demonstrated to also provide better current density control of the electrode due to its high conductivity [28,29]. However, Yihao et al. [30] propose a robust and highly efficient scalable electrode from a crumpled Au-CNT forest. This symmetric supercapacitor has a maximum specific capacitance of 6 mF cm^{-2} at a current density of 40 mA cm^{-2} at large strains, and exhibits superior mechanical and electrochemical stability. This investigation provides a feasible method to synthesize vertically aligned nanotubes or nanowires into highly stretchable supercapacitors for outstanding and robust electrochemical capabilities.

In the present work, we report the synthesis of high performance electrodes based on Au deposited on CNTs. The Au thin films were synthesized by magnetron sputtering on vertically aligned CNTs template using one-step process. The electrochemical measurements reveal that Au@CNTs film shows enhanced properties with higher areal capacitance values compared to those of pure CNTs or Au thin film electrodes in a mild electrolyte of 0.5 M H_2SO_4 and excellent stability over 10 000 cycles.

* Corresponding author.
E-mail address: rog.sabrina@yahoo.fr (S. Roguai).

https://doi.org/10.1016/j.tsf.2023.139894
Received 22 October 2022; Received in revised form 15 May 2023; Accepted 18 May 2023
Available online 20 May 2023

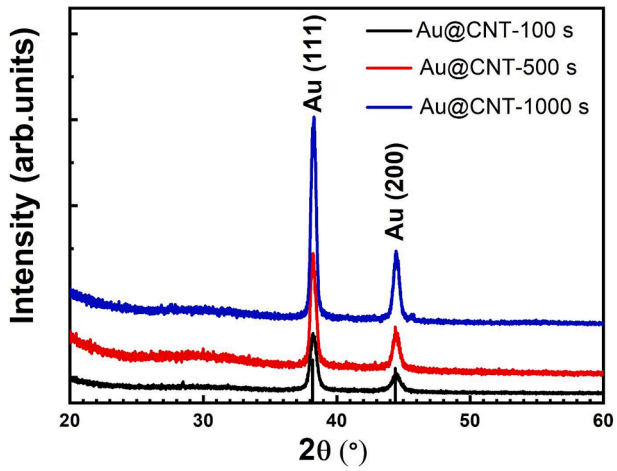

Fig. 1. XRD patterns of Au@CNTs samples deposited for 100 s, 500 s, and 1000 s.

Table 1
Structural parameters D and the ε of different Au@CNTs films, with different time of deposition [100, 500, 1000s], at 50 W power and 0.5 Pa working pressure.

Samples	D (nm)	ε%
Au@CNT-100 s	17	−0.059
Au@CNT-500 s	21	−0.102
Au@CNT-1000 s	23	−0.123

2. Experimental

2.1. Synthesis of vertically aligned CNTs films

The CNTs were grown over (001) oriented silicon substrates coated with a 10 nm thick amorphous carbon layer using plasma enhanced chemical vapor deposition (PECVD) process. A 10 nm thick nickel (Ni) film was deposited via DC-sputtering after which the sample was transferred to the PECVD reactor. Prior to CNT growth, the Ni film was transformed into Ni catalyst nanoparticles (NPs) of ~ 50 nm in diameter, after annealing at 600 °C. The aligned CNTs arrays were grown via PECVD in acetylene (C_2H_2) plasma diluted with ammonia (NH_3) in a 1:3 flow ratio, at a constant substrate temperature of 500 °C. The pressure and power were kept constants under 0.2 Pa and 125 W, respectively. The synthesis time was for a duration of 60 min for all samples.

2.2. Deposition of Au on the CNTs

AuNPs were deposited on the CNTs samples by DC-sputtering in another chamber. The Au target (99.999% in purity and 2 in. in diameter) was sputtered using Ar (flux of 30 sccm) at 50 W power, O.5 Pa working pressure, and the substrates were mounted on a holder and placed at a distance of ~20 cm from the sputtering target, for different deposition times 100, 500 and 1000 s, thus the samples are assigned as Au@CNT-100 s, Au@CNT-500 s and Au@CNT-1000s, respectively.

2.3. Sample characterization

2.3.1. Structural and surface characterization

The morphology of the Au@CNT was investigated using scanning electron microscopy (SEM, on a JEOL JSM 7500 F) with a working distance of 10 mm, acceleration voltage ranging from 0.1 kV to 30 kV, with a resolution of 1.0 nm at 15 kV, 1.4 nm at 1 kV. For transmission electron microscopy (TEM; H9000-NAR operating at 300 kV) was used. Samples were scratched with a diamond tip and collected on a TEM copper grid covered with a thin holey carbon film prior to sample examination. Structural characterization of the samples was performed by X-ray diffraction (XRD) (D8 Advance, Bruker, Germany) with Cu Kα radiation λ= 0.1546 nm radiation and a tube voltage of 40 kV, tube current of 40 mA, the operating power of 16 W, the grazing incidence angle of 1°, scanning speed of 1°/min, and scanning range of 20 °–80 °. The surface chemical analysis was evaluated by X-ray photoelectron spectroscopy (XPS) (Thermo Scientific K-Alpha, Al Kα radiation 1486.68 eV) with a spot size of 250 × 250 μm. Cores levels and survey

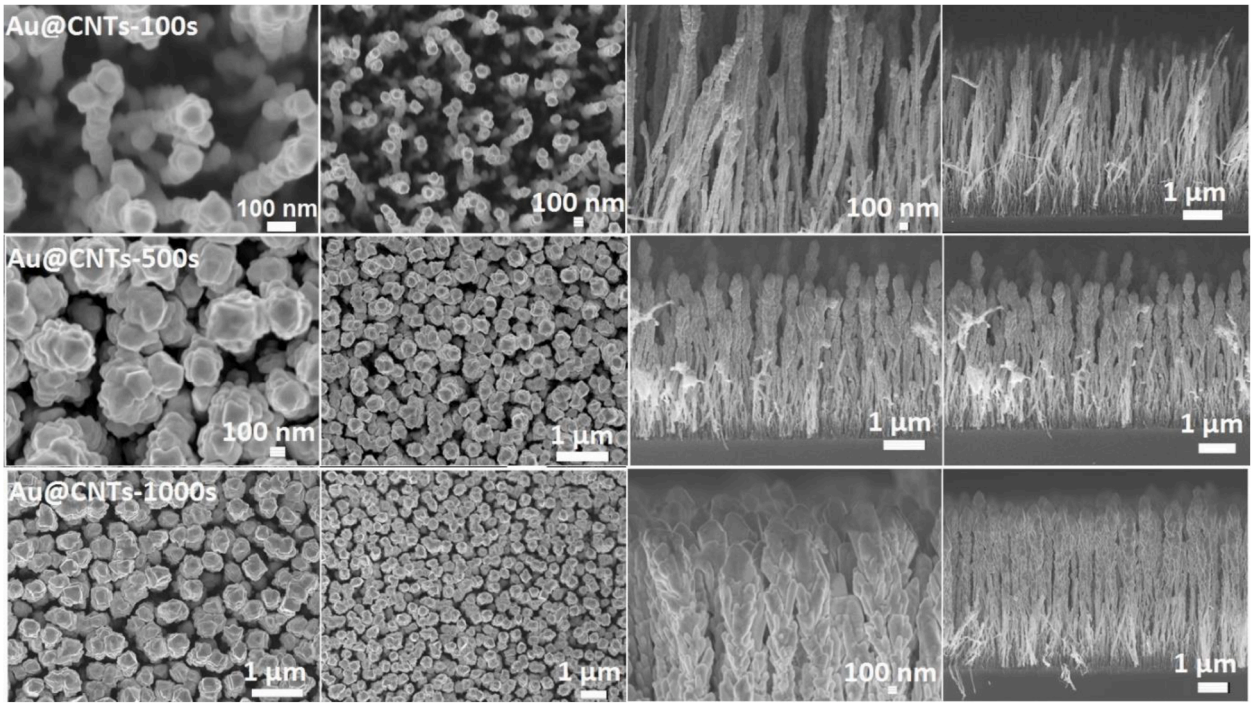

Fig. 2. Top view and cross-section SEM images of Au@CNTs-100 s, Au@CNTs-500 s, and Au@CNTs-1000s films.

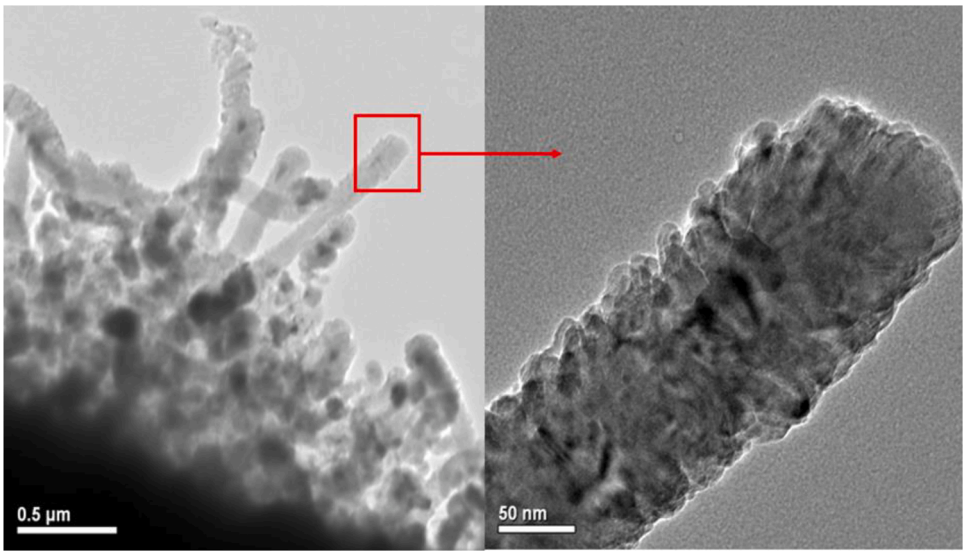

Fig. 3. TEM images of the Au@CNTs deposited for 100 s.

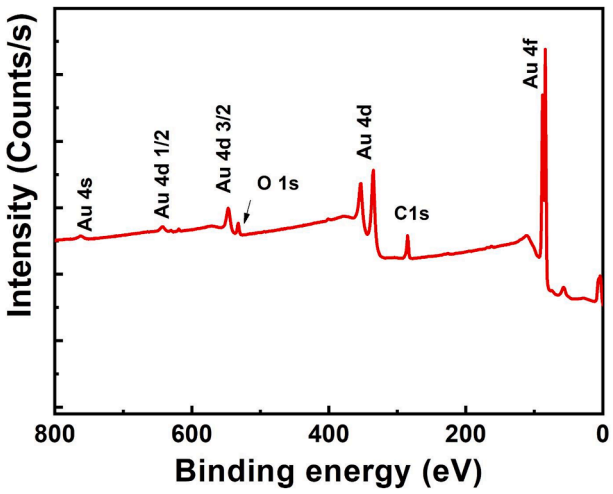

Fig. 4. Representative example of XPS spectra of Au@CNTs-500 s films.

spectra were acquired at 20 and 150 eV, respectively. A flood gun was used for charge compensation. No additional binding energy shift (to C 1 s signal) was required.

2.3.2. Electrochemical characterization

Electrochemical measurement was performed in a three-electrode electrochemical cell at room temperature. Au@CNTs sample, Ag/AgCl and Pt foil were used as working, reference and counter electrodes, respectively. Only Au@CNTs active material was in contact with the electrolyte ($S = 0.5$ cm^2). A silver paste was used to ensure good contact with the current collector made with cooper. The electrodes were evaluated by cyclic voltammetry (CV), and galvanostatic charge-discharge in H_2SO_4 (0.5 M) aqueous solution.

3. Results and discussion

3.1. Structural and microstructural studies

The XRD patterns of the samples are shown in Fig. 1. It was observed that the sputtered Au@CNTs films at various time (100, 500, 1000s) is formed in the structure cubic (Au), characterized by the presence of the peaks (111), and (200) occurred (JCPDS card No. 00–004–0784). The XRD patterns revealed that the intensity of this plane of Au increase with increasing time of deposition.

The evaluation of the cristallites size (D) and the strain (ε) of the Au@CNTs films using the following equations (Eq. (1)) and (Eq. (2)) [31,32]:

$$D = \frac{0.9\lambda}{\beta\cos(\theta)} \quad (1)$$

$$\varepsilon = \frac{\beta}{4\tan\theta} \quad (2)$$

Where λ is the wavelength of the incident X-ray (Cu Kα radiation, λ =1.5418 Å), K is a constant of grating geometry (0.9), β is the width at half height of the spectral lines (FWHM), and θ is the Bragg diffraction peak (in radians). The evaluated values are listed in Table 1, it can be seen that the crystallite size increases of (17, 21, 23 nm) with the time of deposition of the films (100, 500, 1000s) respectively. And also the microstrain of the Au@CNTs sample decreases of (−0.059, −0.102, and −0.123) with the increment of deposition time (100, 500, 1000s) respectively, while the negative signs of the ε values indicate compressive strains. The ε decrease is related to the increase of the particle size, which implies the deposit time affects the structure of obtained films.

SEM observations indicated that the deposition of Au@CNTs was found to be achieved. As it can be seen in Fig. 2, there was no effect on the structure of the carbon nanotube forests, and there were no noticeable changes detected between the SEM images of the samples deposited at different time points (100, 500, 1000s). The enlarged TEM observation of Au@CNTs at 100 s is shown in Fig. 3. revealed that the Au was located on the surface of the carbon nanotube, showing that the Au NPs are about 5 nm. These experimental results confirm that the Au NPs were effectively coated on the vertically aligned CNTs by magnetron sputtering deposition.

The XPS spectra of Au@CNTs are shown in Fig. 4, revealing the presence of the peaks Au 4 s (762 eV), Au $4d_{1/2}$ (641 eV), Au $4d_{3/2}$ (547 eV), O 1 s (532 eV) [33,34], Au 4d, C1s, and Au 4f (84.1 eV) due the presence of the amount of metallic Au [32,34]. The bond O1s At 532.0 ± 0.2 eV the oxygen species has a rather higher binding energy. This species is found to occur on exposures to the oxygen of any length. Some research shows this binding energy on the surface of Au to oxygen in the composition of OH groups or to water [35,36], for the formation of oxygen on a Au surface deposition.

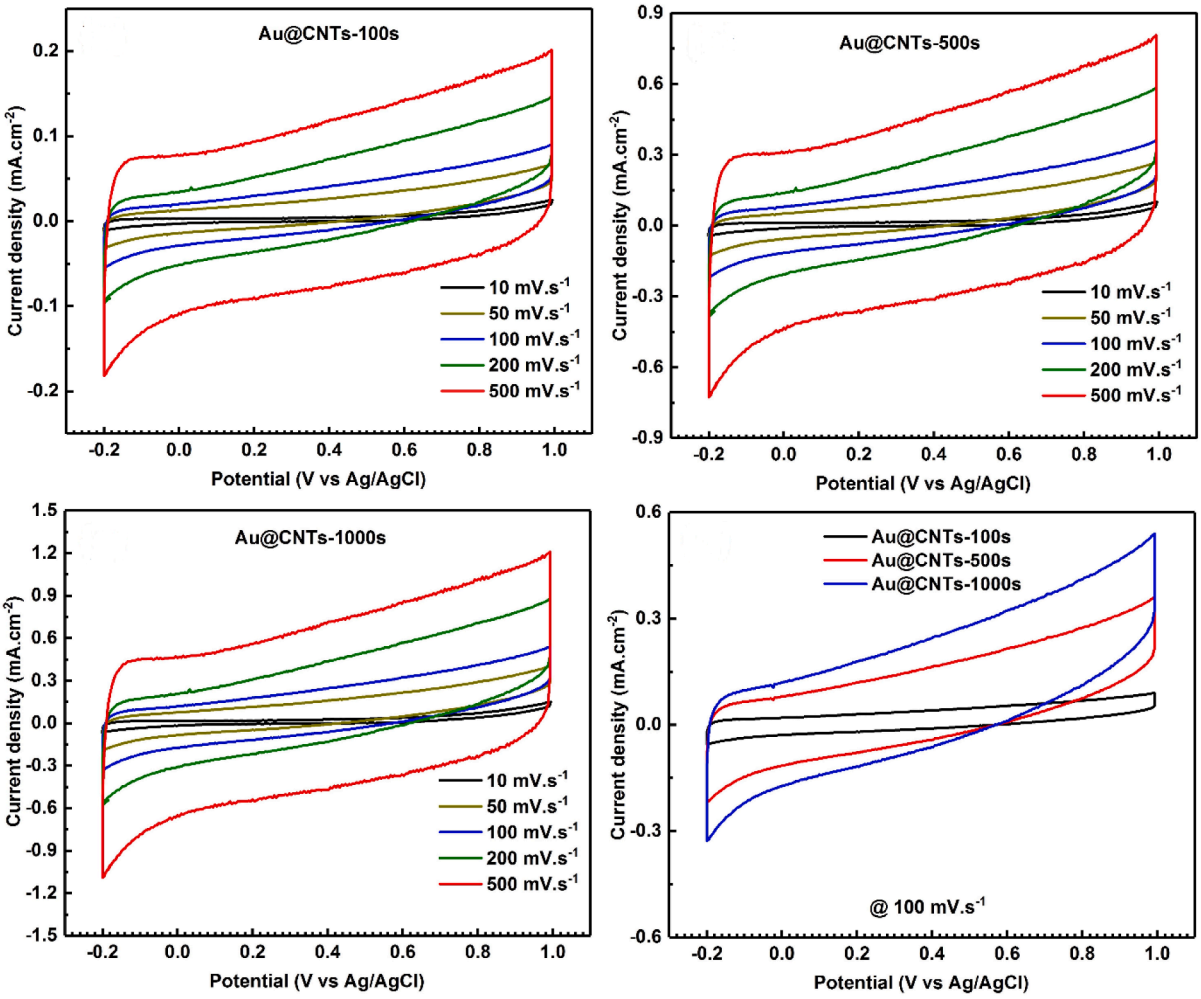

Fig. 5. Electrochemical performance of Au@CNTs films tested in a two-electrode system. CV curves of (a) Au@CNTs (100 s), (b) Au@CNTs (500 s), and (c) Au@CNTs (1000s) films at different scan rates, and (d) comparison CV curves of Au@CNTs (100, 500, 1000s) films at a scan rate of 100 mV/s.

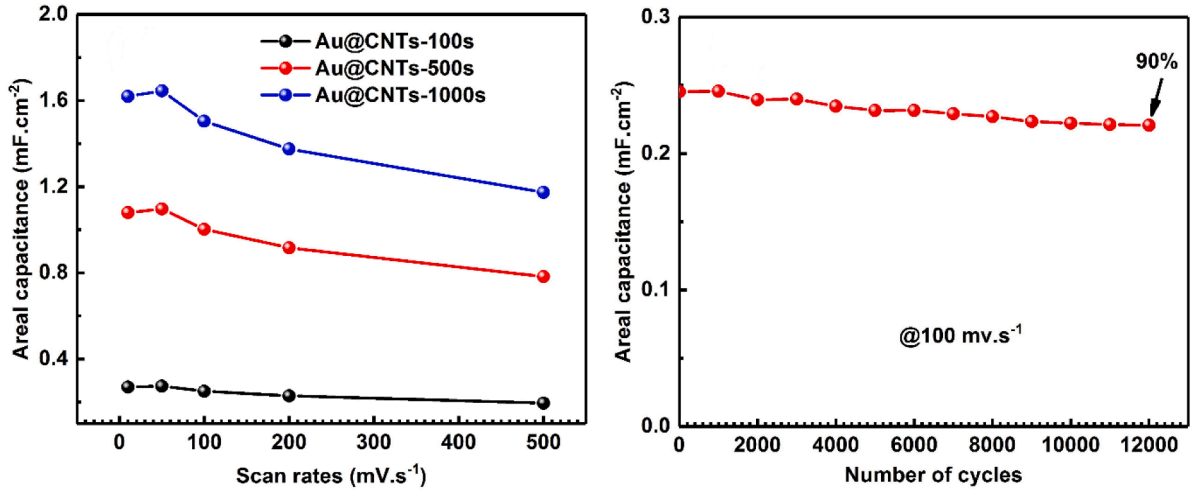

Fig. 6. Areal capacitance as a function of the scan rate curve of Au@CNTs films prepared with different deposition time and cycling stability measured at 100 mV/s for 12.000 cycles of Au@CNTs (100 s) films.

3.2. Electrochemical properties

Fig. 5, represents the CV curves for the electrochemical capacitance of Au@CNTs [100, 500, 1000s] in the potential range of −0.2 V to 1.0 V with scan rates ranging from 10 mV/s to 500 mV/s, of both electrodes in H_2SO_4 solution. The effect of pseudo-capacitance was evident from the cyclic voltammogram for all Au@CNTs samples [100,500, 1000s], as peaks of oxidation and reduction appeared. The separation between the

Table 2
The Areal capacitance of different Au@CNTs films, with different time of deposition [100, 500, 1000s], at 50 W power and 0.5 Pa working pressure.

Scan rates (mV.s^{-1}) The Areal capacitance (mF/cm^2)	Au@CNTs-100 s	Au@CNTs-500 s	Au@CNTs-1000 s
10	0.2699	1.0796	1.6194
50	0.27409	1.0964	1.6445
100	0.25066	1.0026	1.504
200	0.22914	0.91658	1.3749
500	0.1957	0.78279	1.1742

oxidation and reduction potential peaks in the sample became greater, with the reduction potential peaks moving to the left side of the spectrum as the scan rate increased. Fig. 5, shows the comparison of CV curves for the electrochemical capacity of Au@CNTs films [100, 500, 1000s] at 100 mV/s. It can be seen that the deposition of the sample Au@CNTs films [1000s] was faster than that of the other samples Au@CNTs films [100, and 500 s]. As can be seen from the spectra, the CV curves maintain a relatively symmetrical rectangular shape, there is no evident fluctuation until the voltage window is expanded to 1.0 V. At this time, the Au@CNT films present critical capacitive performance, with the CV curve having a clear rectangular shape, which remains stable even at a scan rate of 100 mV/s. At this scan rate, it is possible for the current to respond quickly to the voltage change, suggesting that the electrolyte is able to diffuse through the film quickly. It can be seen that as the deposition time increases, the oxidation–reduction reaction increases, which could be due to the modification of the Au NPs on the CNTs.

As shown in Fig. 6, from CV curves, the areal capacitance (F/cm^2) of Au@CNTs [100, 500, 1000s] at different scan rates is calculated according to the following equation

$$C = \frac{\int idV}{2 \times \Delta V \times v \times A} \quad (3)$$

Where $\int idV$ is the integrated area of CV curves; $\triangle V$ is the scanned potential window, v is the scan rate, and A is the area of the single electrode (cm^2). Were seen that an increased of the values of areal capacitance with a deposition time of 100, 500, 1000s, respectively (see Table 2), as the scan rate reaches 50 mV/s. We noted that the scan rate affects the electron transfer as well as the diffusion of ions from the electrolyte into the electrodes. Usually, there is a decrease in the specific capacitance with increasing scan rate. As illustrated for the Au@CNTs (100 s) films, the areal capacitance remained about 90% of its initial value after 10.000 cycles, which implies excellent capacitive performance and stability (Fig. 6).

The voltammograms recorded during the electrochemical studies of Au@CNTs [100, 500, 1000s] electrode using the CV method by applying potential from −0.2 to 0.6 V at a potential sweep rate of 10 mVs^{-1} are shown in Fig. 7, as a result, the bare Au@CNTs exhibited significant electrochemical activity with increasing deposition time. They displayed considerable redox performance, that is due to the high active surface area of the as-synthesized Au@CNTs, proving the viable electrochemical properties. Further, the surface area of the electrode was suggested to have been enhanced by changing it with deposition time. The more intense signals corresponding to Au@CNTs (1000s) provide a reason for their good conductive characteristics.

As also shown in Fig. 7, the anodic current density, here, it can be seen from the results that the anodic current density (relative to Ag/AgCl) at a scan rate of 10 mVs^{-1} for the Au@CNTs bioanode [100, 500, 1000s] increased from 0.20 $mAcm^2$ Au@CNTs (100 s) to 0.29 mA cm^2 Au@CNTs (1000s), indicating that this anode has a strong potential to achieve the oxidation of H_2SO_4. This rise in current response resulting from H_2SO_4 oxidation may result from the incorporation of Au NPs into CNTs, with the increase in deposition time, which has a noticeable effect in assisting the electron transmission and enhancing the catalytic activity of the Au.

4. Conclusions

Au@CNT [100,500,1000s] films were fabricated by DC-sputtering of Au on vertically aligned CNTs templates. The Au@CNTs electrodes represent a nanostructured morphology. The areal capacitances of the AuN@CNTs electrodes were found to increase as the time of deposition increases. Moreover, the electrodes shows a stability over 10.000 consecutive cycles in 0.5 M H_2SO_4 electrolyte solution.

Under optimized conditions, the Au@CNT (1000 s) electrode exhibits a high areal capacitance of 1.6445 mF cm^{-2} at a scan rate of 50 mV s^{-1} which is higher than Au thin film or CNTs alone. The obtained results suggest that Au@CNTs in particular and porous Au metal in general can compete with other type of materials as a promising material for micro-supercapacitor applications.

Declaration of Competing Interest

The authors declare the following financial interests/personal relationships which may be considered as potential competing interests: Sabrina Roguai reports was provided by Abbes Laghrour University of Khenchela Faculty of Science and Technology. Sabrina Roguai reports a relationship with Abbes Laghrour University of Khenchela Faculty of Science and Technology that includes: employment

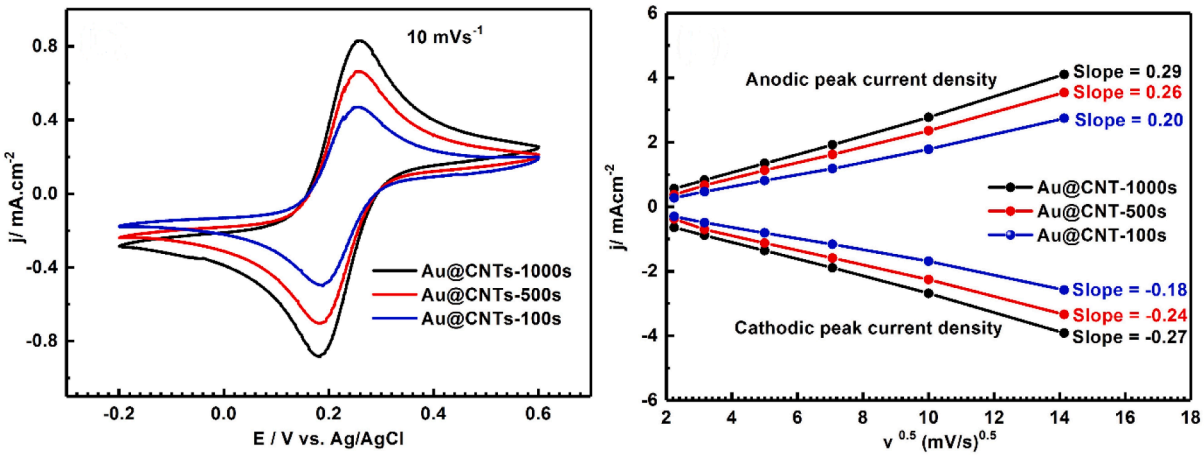

Fig. 7. Cyclic voltammograms measured at10 mVs^{-1} of Au@CNTs films prepared with different deposition time and cyclic voltammetric anodic and cathodic peak current density as the function of the scan rate $(v)^{1/2}$ of Au@CNTs (100, 500, 1000s) films.

Acknowledgments

Funding was provided by the General Direction of research and development technologies/ Ministry of Higher Education and Research Sciences DGRSDT/ MESRS, Algeria. The financial support from Abbes Laghrour University of Khenchela (Algeria). The authors would like to thank the Project (RFU) and LASPI2A Laboratory of Khenchela University (Algeria) for their financial support of this research project.

References

[1] A. Burke, Ultracapacitors: why, how, and where is the technology, J. Power Sources 91 (2000) 37–50, https://doi.org/10.1016/S0378-7753(00)00485-7.
[2] T. Kim, Y.H. Mo, K.S. Nahm, S.M. Oh, Carbon nanotubes (CNTs) as a buffer layer in silicon/CNTs composite electrodes for lithium secondary batteries, J. Power Sources 162 (2006) 1275–1281, https://doi.org/10.1016/j.jpowsour.2006.07.062.
[3] L.L. Zhang, M. Winter, J.O. Besenhard, Carbon-based materials as supercapacitorelectrodes, Chem. Soc. Rev. 38 (2009) 2520–2531, https://doi.org/10.1039/B813846J.
[4] D. Zhang, T. Yan, L. Shi, Z. Peng, X. Wen, J. Zhang, Enhanced capacitive deionization performance of graphene/carbon nanotube composites, J. Mater. Chem. 22 (2012) 14696–14704, https://doi.org/10.1039/C2JM31393F.
[5] B. Jia, L. Zou, Graphene nanosheets reduced by a multi-step process as highperformance electrode material for capacitive deionisation, Carbon N Y 50 (2012) 2315–2321, https://doi.org/10.1016/j.carbon.2012.01.051.
[6] Z. Chen, C. Song, X. Sun, H. Guo, G. Zhu, Kinetic and isotherm studies on the electrosorption of NaCl from aqueous solutions by activated carbon electrodes, Desalination 267 (2011) 239–243, https://doi.org/10.1016/j.desal.2010.09.033.
[7] C.H. Hou, C.Y. Huang, A comparative study of electrosorption selectivity of ions by activated carbon electrodes in capacitive deionization, Desalination 314 (2013) 124–129, https://doi.org/10.1016/j.desal.2012.12.029.
[8] L. Zou, G. Morris, D. Qi, Using activated carbon electrode in electrosorptive deionisation of brackish water, Desalination 225 (2008) 329–340, https://doi.org/10.1016/j.desal.2007.07.014.
[9] S. Porada, R.D. Weingarth, H.V.M. Hamelers, M. Bryjak, V. Presser, P. M. Biesheuvel, Carbon flow electrodes for continuous operation of capacitive deionization and capacitive mixing energy generation, J. Mater. Chem. A 2 (2013) 9313–9321, https://doi.org/10.1039/C4TA01783H.
[10] L. Wang, M. Wang, Z. Huang, T. Cui, X. Gui, F. Kang, K. Wang, D. Wu, Capacitive deionization of NaCl solutions using carbon nanotube sponge electrodes, J. Mater. Chem. 21 (2011) 18295–18299, https://doi.org/10.1039/C1JM13105B.
[11] H. Li, L. Pan, T. Lu, Y. Zhan, C. Nie, Z. Sun, A comparative study on electrosorptive behavior of carbon nanotubes and graphene for capacitive deionization, J. Electroanal. Chem. 653 (2011) 40–44, https://doi.org/10.1016/j.jelechem.2011.01.012.
[12] S. Porada, L. Weinstein, R. Dash, A. van der Wal, M. Bryjak, Y. Gogotsi, P. M. Biesheuvel, Water desalination using capacitive deionization with microporous carbon electrodes, ACS Appl. Mater. Interfaces 4 (2012) 1194–1199, https://doi.org/10.1021/am201683j.
[13] S. Porada, L. Weinstein, M. Oschatz, M. Bryjak, J.S. Atchison, K.J. Keesman, S. Kaskel, P.M. Biesheuvel, Direct prediction of the desalination performance of porous carbon electrodes for capacitive deionization, Energy Environ. Sci. 6 (2013) 3700–3712, https://doi.org/10.1039/C3EE42209G.
[14] C. Huang, J. He, Electrosorptive removal of copper ions from wastewater by using ordered mesoporous carbon electrodes, Chem. Eng. J. 221 (2013) 469–475, https://doi.org/10.1016/j.cej.2013.02.028.
[15] C. Tsouris, R. Mayes, J. Kiggans, K. Sharma, S. Yiacoumi, D. DePaoli, S. Dai, Mesoporous carbon for capacitive deionization of saline water, Environ. Sci. Technol. 45 (2011) 10243–10249, https://doi.org/10.1021/es201551e.
[16] M. Antonietti, N. Fechler, T.P. Fellinger, Carbon aerogels and monoliths: control of porosity and nanoarchitecture via sol-gel routes, Chem. Mater. 26 (2013) 196–210, https://doi.org/10.1021/cm402239e.
[17] M.E. Suss, T.F. Baumann, W.L. Bourcier, C.M. Spadaccini, K.A. Rose, J.G. Santiago, M. Stadermann, Capacitive desalination with flow-through electrodes, Energy Environ. Sci. 5 (2012) 9511–9519, https://doi.org/10.1039/C2EE21498A.
[18] J.C. Farmer, D.V. Fix, G. Mack, R.W. Pekala, J.F. Poco, Capacitive deionization of NaCl and NaNO3 solutions with carbon aerogel electrodes, J. Electrochem. Soc. 143 (1996) 159, https://doi.org/10.1149/1.1836402.
[19] A.J.S. Ahammad, J.J. Lee, M.A. Rahman, Electrochem. Sens. Based Carbon Nanotubes Sens. 9 (2009) 2289–2319, https://doi.org/10.3390/s90402289.
[20] P.M. Ajayan, Nanotubes from carbon, Chem. Rev. 99 (1999) 1787–1800.
[21] R. Burge, B. Dawson-Hughes, D.H. Solomon, J.B. Wong, A. King, A. Tosteson, Incidence and economic burden of osteoporosis-related fractures in the United States, 2005–2025†, J. Bone Mineral Res. 22 (2007) 465–475, https://doi.org/10.1359/JBMR.061113.
[22] N. Saito, Y. Usui, K. Aoki, N. Narita, M. Shimizu, K. Hara, N. Ogiwara, K. Nakamura, N. Ishigaki, H. Kato, S. Taruta, M. Endo, M, Carbon nanotubes: biomaterial applications, Chem. Soc. Rev. 38 (2009) 1897–1903, https://doi.org/10.1039/B804822N.
[23] D. Tasis, N. Tagmatarchis, A. Bianco, M. Prato, Chemistry of Carbon Nanotubes, Chem. Rev. 106 (2006) 1105–1136, https://doi.org/10.1021/cr050569o.
[24] Y.H. Yun, Z. Dong, V.N. Shanov, A. Doepke, W.R. Heineman, H.B. Halsall, A. Bhatta charya, D.K.Y. Wong, M.J. Schulz, Fabrication and characterization of carbon nanotube array electrodes with gold nanoparticle tips, Sens. Actuators B: Chem. 133 (2008) 208–212, https://doi.org/10.1016/j.snb.2008.02.019.
[25] Ch. Cao, Y. Zhou, S. Ubnoske, J. Zang, Y. Cao, Ph. Henry, Ch.B. Parker, J.T. G.lass, Highly stretchable supercapacitors via crumpled vertically aligned carbon nanotube forests, Adv. Energy Mater. 9 (22) (2019), 1900618, https://doi.org/10.1002/aenm.201900618, 2019.
[26] Sh. Zu, J. Sheng, J. Ni, Y. Li, 3D vertical arrays of nanomaterials for microscaled energy storage devices, Acc. Mater. Res. 2 (2021) 1215–1226, https://doi.org/10.1021/accountsmr.1c00175.
[27] J.C. Love, L.A. Estroff, J.K. Kriebel, R.G. Nuzzo, G.M. Whitesides, Self-assembled monolayers of thiolates on metals as a form of nanotechnology, Chem. Rev. 105 (2005) 1103–1170, https://doi.org/10.1021/cr0300789.
[28] Y. Yun, Z. Dong, V.N. Shanov, M.J. Schulz, Electrochemical impedance measurement of prostate cancer cells using carbon nanotube array electrodes in a microfluidic channel, Nanotechnology 18 (2007), 465505, https://doi.org/10.1088/0957-4484/18/46/465505.
[29] R. Anandhi, R. Mohan, K. Swaminathan, K. Ravichandran, Superlattice, Influence of aging time of the starting solution on the physical properties of fluorine doped zinc oxide films deposited by a simplified spray pyrolysis technique, Microst 51 (2012) 680–689, https://doi.org/10.1016/j.spmi.2012.02.006.
[30] Zhou et al Y. Zhou, Ch. Cao, Y. Cao, Q. Han, Ch.B. Parker, J.T. G.lass, Robust and high-performance electrodes via crumpled Au-CNT forests for stretchable supercapacitors, Matter 2 (5) (2020) 1307–1323, https://doi.org/10.1016/j.matt.2020.02.
[31] S. Roguai, A. Djelloul, Structural, microstructural and photocatalytic degradation of methylene blue of zinc oxide and Fe-doped ZnO nanoparticles prepared by simple coprecipitation method, Solid State Commun. 334–335 (2021), 114362, https://doi.org/10.1016/j.ssc.2021.114362.
[32] B.Y.P.G. Jones, H. Rumpel, E. Schwarzmann, G.M. S.heldrick, Gold(III) oxide, Acta. Crystallogr. Sect. B 35 (1979) 1435–1437, https://doi.org/10.1107/S0567740879006622.
[33] H. Shi, R. Asahi, C. Stampfl, Properties of the gold oxides Au2O3 and Au2O: first-principles investigation, Phys. Rev. B 75 (2007) 205125–205133, https://doi.org/10.1103/PhysRevB.75.205125.
[34] K. Juodkazias, J. Juodkazyte, V. Jasulaitiene, A. Lukinskas, B. Sebeka, XPS studies on the gold oxide surface layer formation, Electrochem. Commun. 2 (2000) 503–507, https://doi.org/10.1016/S1388-2481(00)00069-2.
[35] E. Irissou, M.C. D.enis, M. Chaker, D. Guay, Gold oxide thin film grown by pulsed laser deposition in an O2 atmosphere, Thin Solid Films 472 (2005) 49–57, https://doi.org/10.1016/j.tsf.2004.06.092 (2005).
[36] B. Koslowski, H.-.G. Boyen, C. Wilderotter, G. Kastle, P. Ziemann, R. Wahrenburg, P. Oelhafen, Oxidation of preferentially (1 1 1)-oriented Au films in an oxygen plasma investigated by scanning tunneling microscopy and photoelectron spectroscopy, Surf. Sci. 475 (2001) 1–10, https://doi.org/10.1016/S0039-6028(00)00986-9.